Molecular Simulation of Phase Equilibria for Water−*n*-Butane and Water−*n*-Hexane Mixtures

Georgios C. Boulougouris,[†,‡] Jeffrey R. Errington,[§,||] Ioannis G. Economou,[†] Athanassios Z. Panagiotopoulos,*[,§] and Doros N. Theodorou[†,⊥]

Molecular Modeling of Materials Laboratory, Institute of Physical Chemistry, National Research Center for Physical Sciences "Demokritos", GR-15310 Aghia Paraskevi Attikis, Greece, Department of Chemical Engineering, National Technical University of Athens, GR-15773 Zografos, Athens, Greece, Institute for Physical Science and Technology and Department of Chemical Engineering, University of Maryland, College Park, Maryland 20742, and Department of Chemical Engineering, University of Patras, GR-26500 Patras,Greece

Received: November 16, 1999; In Final Form: March 13, 2000

Monte Carlo simulations were performed to obtain the Henry's law constants of *n*-butane and *n*-hexane in water and of water in *n*-hexane at different temperatures. Literature intermolecular potential functions optimized to the pure component vapor−liquid coexistence properties were used for the calculations. The Widom test-particle insertion technique was used for the infinite dilution properties of water in *n*-hexane. This methodology becomes impractical for large solute molecules in dense solvents. A combination of Widom insertions of a small weakly interacting molecule and expanded ensemble simulations was used to determine the Henry's law constants of *n*-butane and *n*-hexane in water. As the hydrocarbon size increased, simulation results were found to deviate from experimental data. These deviations are likely due to limitations of the potential models employed.

Introduction

The phase behavior of water−hydrocarbon mixtures is important in biology, chemistry, physics, and chemical engineering. Most biological systems are aqueous mixtures in which many of the complex dissolved molecules contain hydrocarbon segments. The considerable difference in polarity between water and hydrocarbons results in highly nonideal mixture properties, such as very low mutual solubilities. The optimum design and operation of many processes in the petroleum and petrochemical industry and in environmental technology also require accurate knowledge of the phase equilibria of water−hydrocarbon mixtures.

Recent advances in molecular simulation methodologies have enabled the calculation of thermodynamic properties and phase equilibria of complex fluids.[1] For simulations to reproduce accurately the actual property values, a realistic description of the intermolecular and intramolecular interactions is necessary. Potential models for components such as water,[2,3] carbon dioxide,[4] normal[5−7] and branched[8] alkanes, α-olefins,[9] and others[10] have been developed that reproduce pure component vapor−liquid equilibrium properties and critical constants with good accuracy. Many of these potential models were used for phase equilibrium predictions of nonideal mixtures; in many cases, results were found to be in good agreement with experimental data.[11,12]

In a recent paper, the phase equilibria of water−methane and water−ethane mixtures over a wide temperature and pressure range were obtained from Monte Carlo simulations.[13] The Henry's law constants of the two hydrocarbons in water were evaluated from Widom test-particle insertions. Results at low pressures were in good agreement with experimental data. Gibbs ensemble Monte Carlo (GEMC) simulations at higher pressures agreed with experimental data within a factor of 2, which is comparable to the accuracy of the best phenomenological equations of state available.

In this work, the phase equilibria of water with two higher hydrocarbons, *n*-butane and *n*-hexane, were calculated for a range of temperatures. The solubility of normal alkanes in water is very low and is usually described through the Henry's law constant. Calculations by simulation of the solubility of hydrocarbons in water are quite challenging. As the hydrocarbon chain length increases beyond ethane, direct test-particle insertions become impractical, because of the high density and strong interactions in liquid water. However, gradual insertion of a test molecule is still possible. Such a methodology was used in this work; it consists of a combination of Widom insertions and expanded ensemble (EE)[14−16] techniques. It was shown that this approach provides statistically reliable results for higher hydrocarbons.

The potential model used for all three components is based on the Buckingham exponential-6 (exp-6) functional form for the nonbonded interactions, rather than the more widely used Lennard-Jones model. The exp-6 is a three-parameter model and was shown to be more accurate for pure water and *n*-alkanes than the two-parameter Lennard-Jones model.[3,7] Lorentz−Berthelot combining rules were used to obtain the interactions between unlike groups. In addition, Kong combining rules[17] for unlike pairs were tested for a few state points. In all cases, simulation results were found to be in qualitative agreement with experimental data. Deviations between simulation results and experimental data are likely to be due to deficiencies in

* To whom correspondence should be addressed. E-mail: thanos@ipst.umd.edu.
† National Research Center for Physical Sciences "Demokritos".
‡ National Technical University of Athens.
§ University of Maryland.
|| Current address: Department of Chemical Engineering, Princeton University, Princeton, NJ 08544.
⊥ University of Patras.

10.1021/jp994063j CCC: $19.00
Published on Web 04/27/2000

TABLE 1: Intermolecular Potential Parameters for the Components Studied in This Work

model parameter	water	CH_3	CH_2
ϵ/k_B (K)	159.78	129.6	73.5
σ (Å)	3.195	3.679	4.00
α	12	16	22

the relatively simple pure component intermolecular potential models used.

Potential Models

The potential models for water,[3] *n*-butane, and *n*-hexane[7] used in this work are based on the pairwise-additive exp-6 representation of the nonbonding interactions. The pure component potential development was performed in previous studies[3,7] so as to optimize the representation of thermodynamic properties of the fluid state and, in particular, the vapor−liquid-phase envelope and critical parameters. For water, a known deficiency of the model is the poor representation of the oxygen−oxygen pair correlation functions.[3] The Buckingham exp-6 intermolecular potential function[18] is used in these models.

$$u(t) = \begin{cases} \dfrac{\epsilon}{1-6/\alpha}\left[\dfrac{6}{\alpha}\exp\left(\alpha\left[1-\dfrac{r}{r_m}\right]\right)-\left(\dfrac{r_m}{r}\right)^6\right], & \text{for } r > r_{max} \\ \infty & \text{for } r < r_{max} \end{cases} \quad (1)$$

In eq 1, ϵ, r_m, and α are exp-6 parameters and r is the separation distance between united-atom groups. Parameter r_m is the radial distance at which the exp-6 potential has a minimum. The cutoff distance r_{max} is the smallest positive value for which $du(r)/dr = 0$ and is obtained by the iterative solution of eq 1. The reason a cutoff distance is required is that, at very short distances, the original Buckingham exponential-6 potential becomes negative. Whereas canonical ensemble Monte Carlo or molecular dynamics simulations never sample the unphysical attractive region, this is not the case for trial insertions. The radial distance for which $u(r) = 0$, denoted by σ, can also be computed from eq 1.

In the case of water, a standard Coulombic term is added to the potential. A point charge of $-2q$ ($q = 0.3687e$) is placed at the oxygen center (which coincides with the exp-6 site), and point charges of $+q$ are placed at each of the two hydrogen sites located 1.0668 Å from the oxygen site. The H−O−H angle is 109.5°. Parameter values were optimized to the vapor−liquid coexistence curve and the critical properties of the pure compounds[3,7] and are summarized in Table 1. Bond lengths in the hydrocarbon molecules were fixed to the following values: CH_3-CH_3 = 1.839 Å, CH_3-CH_2 = 1.687 Å, and CH_2-CH_2 = 1.535 Å. The bond-bending angles in these molecules were generated according to the potential

$$u_{bend}(\theta) = \frac{K_\theta}{2}(\theta - \theta_{eq})^2 \quad (2)$$

where K_θ = 62 500 K/rad^2 and $\theta_{eq} = 114°$. Finally, the torsion angles were described by the potential

$$u_{tor}(\varphi) = V_0 + \frac{V_1}{2}(1+\cos\varphi) + \frac{V_2}{2}(1-\cos 2\varphi) + \frac{V_3}{2}(1+\cos 3\varphi) \quad (3)$$

where $V_0 = 0$, V_1 = 355.03 K, V_2 = −68.19 K, and V_3 = 791.32 K.

To calculate the nonbonding interactions between unlike groups belonging to like molecules, or unlike molecules in the case of a mixture, appropriate combining rules should be set. For the case of groups belonging to like molecules, the widely used Lorentz−Berthelot combining rules were used.

$$\epsilon_{ij} = \sqrt{\epsilon_{ii}\epsilon_{jj}} \quad (4)$$

$$\sigma_{ij} = \frac{\sigma_{ii}+\sigma_{jj}}{2} \quad (5)$$

$$\alpha_{ij} = \sqrt{\alpha_{ii}\alpha_{jj}} \quad (6)$$

For the case of groups belonging to unlike molecules, two different combining rules were tested. In one case, all state points were simulated using the Lorentz−Berthelot combining rules. In addition, a limited number of state points were simulated using the combining rules proposed by Kong.[17]

$$\left[\frac{\epsilon_{ij}\alpha_{ij}\exp(\alpha_{ij})}{(\alpha_{ij}-6)\sigma_{ij}}\right]^{2\sigma_{ij}/\alpha_{ij}} = \left[\frac{\epsilon_{ii}\alpha_{ii}\exp(\alpha_{ii})}{(\alpha_{ii}-6)\sigma_{ii}}\right]^{\sigma_{ii}/\alpha_{ii}}\left[\frac{\epsilon_{jj}\alpha_{jj}\exp(\alpha_{jj})}{(\alpha_{jj}-6)\sigma_{jj}}\right]^{\sigma_{jj}/\alpha_{jj}} \quad (7)$$

$$\left[\frac{\epsilon_{ij}\alpha_{ij}\sigma_{ij}^6}{(\alpha_{ij}-6)}\right] = \left[\frac{\epsilon_{ii}\alpha_{ii}\sigma_{ii}^6}{(\alpha_{ii}-6)}\frac{\epsilon_{jj}\alpha_{jj}\sigma_{jj}^6}{(\alpha_{jj}-6)}\right]^{1/2} \quad (8)$$

$$\frac{\sigma_{ij}}{\alpha_{ij}} = \frac{1}{2}\left[\frac{\sigma_{ii}}{\alpha_{ii}}+\frac{\sigma_{jj}}{\alpha_{jj}}\right] \quad (9)$$

These combining rules were shown to provide more accurate results than the Lorentz−Berthelot combining rules for the unlike-pair interactions between nonpolar molecules that have large differences in size and/or potential strength.[17]

Simulation Methodology

The focus of this work is on the infinite dilution properties of *n*-butane and *n*-hexane dissolved in water and of water dissolved in *n*-hexane. In all cases, the pure solvent was simulated initially in the *NpT* (isothermal−isobaric) ensemble. Simulations were performed at different temperatures and at pressure values approximately 10−25% above the solvent vapor pressure at the specific temperature. For relatively low temperatures, where the solvent vapor pressure is well below 0.1 MPa, the pressure was set equal to 0.1 MPa. A constant number of 200 solvent molecules was used for all systems. Long-range Coulombic interactions were calculated through the Ewald summation method.[19] For the Fourier space term, a *k*-vector cutoff of $k^2 < 25$ was used, which resulted in a total of 484 *k*-vectors. The real-space energy was calculated as $\mathrm{erfc}(\lambda r/L)/r$, where L is the simulation box length and λ is a dimensionless number set equal to 5.6. Furthermore, "conducting" boundary conditions were used, i.e., the box was embedded in a medium with infinite dielectric constant. For the exponential-6 long-range corrections, the method of Theodorou and Suter[20] was employed. To determine uncertainties, five separate simulations were completed for each state point.

The objective of our calculations was to determine the difference in excess chemical potential between a molecule in the ideal gas (IG) state and a molecule dissolved in a solvent at infinite dilution. A combination of techniques was used to find this difference. For the calculations, a parameter γ was introduced that scales the full Hamiltonian of the solute

according to the expressions

$$\epsilon_i = \gamma_i \epsilon_{\text{solute}} \tag{10}$$

$$\sigma_i = \gamma_i^{1/3} \sigma_{\text{solute}} \tag{11}$$

$$\alpha_i = \alpha_{\text{solute}} \tag{12}$$

The parameter γ takes values in the interval [0,1], where for $\gamma = 1$, the full potential is used, and for $\gamma = 0$, there is no interaction between the solute molecule and the solvent. The following steps were used to transform the molecule from the IG state to a solute at infinite dilution:

1. Change from a full molecule ($\gamma = 1$) in the IG state to a weak molecule ($\gamma = \gamma_W$) in the IG state.

2. Change from a weak molecule in the IG state to a weak molecule in solution.

3. Change from a weak molecule in solution to a full molecule in solution.

The excess chemical potential difference for step 1 was found using configurational bias Widom insertions of full and weak molecules into an empty box of infinite volume. Widom insertions of chain molecules into an empty box provide the excess chemical potential difference between full or weak molecules in the IG state and molecules in the IG state in which the intramolecular nonbonded interactions in a molecule are turned off. Because the latter is the same for both full and weak molecules, the excess chemical potential difference between a full and a weak molecule is the difference between the two Widom insertion results.

$$\beta \Delta\mu_1^{\text{ex}} = -\ln\langle W_{\text{IG}}^{\text{ext}}(\gamma = \gamma_W)\rangle + \ln\langle W_{\text{IG}}^{\text{ext}}(\gamma = 1)\rangle \tag{13}$$

where $W_{\text{IG}}^{\text{ext}}$ represents the normalized Rosenbluth factor[21] of an isolated chain. For the Widom insertions, the energy was separated into internal and external contributions. The internal energy included bond-bending and torsion energies, whereas the external energy included all intramolecular nonbonded interactions and intermolecular alkane−water interactions. Internal interactions were used to generate trial conformations. For each insertion, the normalized Rosenbluth factor, W^{ext}, was determined, where only the external energy was used to calculate W^{ext}.

Widom insertions were also used to calculate the excess chemical potential difference for step 2. Again, two Widom insertions were required, one of a weak chain into the solvent and another of a weak chain into an empty box. The excess chemical potential difference was evaluated as follows:

$$\beta \Delta\mu_2^{\text{ex}} = -\ln \frac{\langle V W_{\text{sol}}^{\text{ext}}(\gamma = \gamma_W)\rangle}{\langle V\rangle} + \ln\langle W_{\text{IG}}^{\text{ext}}(\gamma = \gamma_W)\rangle \tag{14}$$

where V is the instantaneous volume of the simulation cell during an *NpT* simulation. For further information about the Widom insertions, please refer to the detailed discussion in ref 21.

As the size of the solute molecule increases, the Widom insertion technique becomes impractical, because of the difficulty in sampling important configurations. An alternative methodology based on the expanded ensemble (EE) has been proposed.[14−16] Previous calculations for the μ^{ex} value of methane dissolved in water with the two methods agreed well. At 300 K, μ^{ex} was calculated to be 8.53 ± 0.45 kJ/mol using the Widom insertion method[13] and 9.0 ± 0.6 kJ/mol using the EE technique.[16] Given the success of EE techniques in previous studies, the EE method was adopted to calculate the excess chemical potential difference of step 3. The calculations were performed in a manner similar to that of Lyubartsev et al.[16] and Errington and Panagiotopoulos.[10] An *NpT* Monte Carlo simulation was performed with N water molecules and one hydrocarbon molecule. Throughout a simulation, a given number of sub-ensembles was sampled. In each sub-ensemble the solute interacted with the solvent with a different Hamiltonian (different value of the parameter γ). During the simulation, attempts were made to move from one sub-ensemble to another. The frequency with which each sub-ensemble was visited was dictated by the free energy of the Hamiltonian. To sample each Hamiltonian with equal frequency, weighting functions were introduced. An attempt to move from sub-ensemble i to j was accepted with probability

$$P_{i\to j} = \min\left[1, \frac{\omega_j}{\omega_i}\exp\{-\beta(U(\gamma_j) - U(\gamma_i))\}\right] \tag{15}$$

where $U(\gamma_i)$ and ω_i are the energy and weight of Hamiltonian i, respectively. The weights were adjusted prior to the production phase of the simulation so that each sub-ensemble was visited with approximately the same frequency. Throughout the simulation, the probability distribution of visiting a given sub-ensemble was collected. The difference in the excess chemical potential of Hamiltonians i and j was evaluated by the expression

$$\beta\mu^{\text{ex}}(\gamma_j) - \beta\mu^{\text{ex}}(\gamma_i) = -\ln\left(\frac{p_j}{p_i}\right) + \ln\left(\frac{\omega_j}{\omega_i}\right) \tag{16}$$

where p_i is the probability of visiting sub-ensemble i. The total excess chemical potential change for step 3 was taken as the sum of the differences between adjacent sub-ensembles.

$$\beta \Delta\mu_3^{\text{ex}} = \sum_i [\beta\mu^{\text{ex}}(\gamma_{i+1}) - \beta\mu^{\text{ex}}(\gamma_i)] \tag{17}$$

Finally, the total difference in excess chemical potential between a molecule in the IG state and a molecule dissolved in a solvent at infinite dilution was determined from

$$\beta\mu_{\text{solute}}^{\text{ex}} = \ln\langle W_{\text{IG}}^{\text{ext}}(\gamma = 1)\rangle - \ln + \frac{\langle V W_{\text{sol}}^{\text{ext}}(\gamma = \gamma_W)\rangle}{\langle V\rangle} \sum_i [\beta\mu^{\text{ex}}(\gamma_{i+1}) - \beta\mu^{\text{ex}}(\gamma_i)] \tag{18}$$

where the first γ_i was equal to γ_W, and the last γ_i was equal to 1. Subsequently the Henry's law constant was calculated from the expression

$$H_{\text{solute}\to\text{solvent}} = \lim_{x_{\text{solute}}\to 0}\left[\frac{\rho_{\text{solvent}}}{\beta}\exp(\beta\mu_{\text{solute}}^{\text{ex}})\right] \tag{19}$$

For the case of *n*-butane in water, the first term in eq 18 was zero because of the fact that *n*-butane does not have any intramolecular nonbonded interactions. The Rosenbluth factor $W_{\text{sol}}^{\text{ext}}$ was determined using a total of (50−100) × 10^6 Monte Carlo steps, in which 15% of the moves were test-particle insertions. At 300 K, a value of $\gamma_W = 1$ was used, whereas at 340, 390, and 460 K, the value of γ_W was set to 0.3. The EE runs consisted of seven sub-ensembles, which sampled the following ranges of the parameter γ: 0.1−0.4, 0.3−0.6, 0.5−0.8, and 0.7−1.0. With this selection, there were three points of overlap between two different sets of EE runs. The free

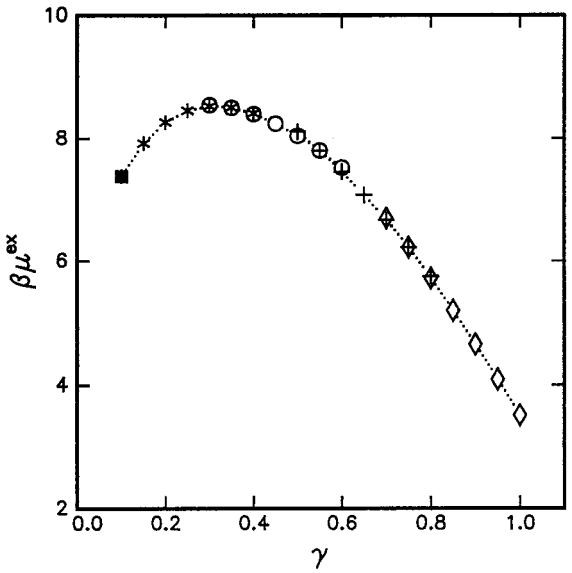

Figure 1. Free energy of inserting *n*-butane into water at 300 K as a function of the parameter γ. A filled square represents the Widom insertion. Asterisks, open circles, crosses, and open diamonds are used for the EE simulations in the ranges 0.1−0.4, 0.3−0.6, 0.5−0.8, and 0.7−1.0, respectively.

energy difference between overlapping sets was taken as the average difference between the three common points.

For *n*-hexane in water, all terms in eq 18 had to be evaluated. The Rosenbluth factor W_{IG}^{ext} was determined using 1×10^6 test-particle insertions. The Rosenbluth factor W_{sol}^{ext} was determined using a total of $(50-100) \times 10^6$ Monte Carlo steps, in which 15% of the moves were test-particle insertions. Widom insertions of *n*-hexane molecules were performed for $\gamma_W = 1$ at 300 K; for $\gamma_W = 0.15$ at 340, 370, 405, and 450 K; and for $\gamma_W = 0.3$ at 500 K. Two sets of EE runs were used, which sampled the following ranges of the parameter γ: $\gamma_W = 0.1 - 0.5$ and $0.5 - 1$. At 300 K, a total number of 200×10^6 Monte Carlo steps was performed. As the temperature increased, a smaller number of steps were attempted, specifically, 120×10^6 at 340 K and 20×10^6 for each of the remaining temperatures.

For water in *n*-hexane, EE simulations were not required. Good statistics were obtained using Widom insertions of full water molecules. In addition, water does not have any nonbonded intramolecular interactions; hence, only the second term of eq 18 had to be evaluated. To determine the excess chemical potential, a total of 10×10^6 Monte Carlo steps were attempted, in which 15% of the moves were insertion attempts.

Results and Discussion

The Henry's law constant of *n*-butane in water was calculated using a combination of Widom insertions and EE simulations, as explained above. In Figure 1, $\beta\mu^{ex}(\gamma)$ is shown as a function of the parameter γ for the insertion of *n*-butane in water at 300 K. The value for $\gamma = 0.1$ was obtained from Widom insertions. The shape of the curve is typical for all of the temperatures examined. It reaches a maximum at relatively low γ values and then decreases. A thorough investigation is necessary in order to optimize the EE part of the calculation (number of EE sets, discretization of γ space, overlap between different EE sets, etc.). Preliminary calculations using a higher discretization of γ space for the same number of total moves in the simulation provided no improvement in the statistics.

The μ^{ex} value and the Henry's law constant of *n*-butane in water were calculated at 300, 340, 390, and 460 K, and results are shown in Table 2. Simulation results for the Henry's constant are compared against experimental data[22] in Figure 2. Calculations are in reasonable agreement with experimental data, considering the statistical uncertainty in the simulations and the scatter in the experimental data (not shown in Figure 2). The simulation predicts accurately the maximum in the Henry's constant at approximately 373 K. Nevertheless, simulation values at 340, 390, and 460 K are lower than the experimental data by approximately 2500 MPa. The solid line shown in Figure 2 was based on the correlation of five different experimental data sets in the temperature range 298−513 K.[22] For a given temperature, the deviation between the different measurements of Henry's constant was as much as 6000 MPa.[22]

TABLE 2: Simulation Results for μ^{ex} and the Henry's Law Constant of *n*-butane in Water

temperature (K)	pressure (MPa)	μ^{ex} (kJ/mol)	Henry's constant (MPa)
300	0.10	8.8 ± 1.5	4600 ± 2800
340	0.10	10.5 ± 1.2	6200 ± 2600
390	0.19	12.1 ± 1.2	6900 ± 2600
460	1.14	11.0 ± 1.1	3200 ± 1000

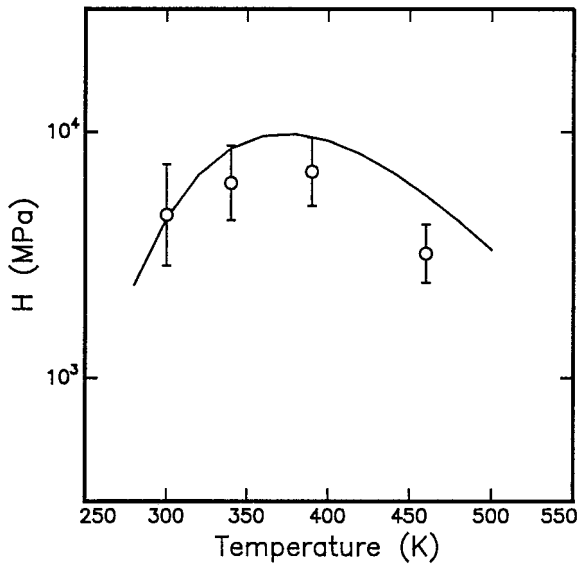

Figure 2. Henry's law constant of *n*-butane in water. Experimental data (solid line)[22] and Monte Carlo simulation using the novel methodology that combines Widom insertion and EE techniques (points).

Simulation results for the μ^{ex} value and the Henry's constant of *n*-hexane in water are presented in Table 3. In Figure 3, simulations for the Henry's constant are compared against experimental data.[23] Simulation results are in qualitative agreement with experimental data, predicting an increase in the Henry's constant up to approximately 370 K and then a decrease. However, for all of the temperatures examined (except 500 K), the calculated values are well below the experimental measurements by a factor of approximately 2−3, depending on the temperature. In other words, simulation predicts that *n*-hexane is more soluble in water than it is in reality. A similar behavior was calculated for cyclohexane in water.[10] Such inaccuracy should be attributed to the approximate nature of the potential model used in all of these calculations, both for water and for the hydrocarbons. Although the pairwise intermolecular potential provides accurate predictions of pure component phase behavior over a wide temperature and pressure range that includes the critical parameters, it becomes progressively inaccurate for highly nonideal asymmetric mixtures. For example, the pairwise

TABLE 3: Simulation Results for μ^{ex} and the Henry's Law Constant of *n*-hexane in Water

temperature (K)	pressure (MPa)	μ^{ex} (kJ/mol)		Henry's constant (MPa)	
		Lorentz−Berthelot	Kong	Lorentz−Berthelot	Kong
300	0.10	8.3 ± 0.8		3900 ± 1000	
340	0.10	11.1 ± 1.6		7700 ± 3800	
370	0.10	13.3 ± 1.1		12200 ± 3900	
405	0.29	13.4 ± 1.6		9000 ± 4000	
450	1.00	13.1 ± 1.5	14.1 ± 1.4	6000 ± 2400	7700 ± 2800
500	2.52	11.6 ± 0.7		3000 ± 500	

TABLE 4: Simulation Results for μ^{ex} and the Henry's Law Constant of Water in *n*-hexane

temperature (K)	pressure (MPa)	μ^{ex} (kJ/mol)		Henry's constant (MPa)	
		Lorentz−Berthelot	Kong	Lorentz−Berthelot	Kong
300	0.10	−1.14 ± 0.11		11.9 ± 0.8	
340	0.11	−0.64 ± 0.12	0.13 ± 0.13	16.1 ± 0.9	21.1 ± 1.0
370	0.28	−0.35 ± 0.09		18.7 ± 0.6	
405	0.65	−0.27 ± 0.07		19.7 ± 0.5	
450	1.58	−0.12 ± 0.06	0.38 ± 0.08	20.4 ± 0.4	23.3 ± 0.4
500	3.38	−0.06 ± 0.09		18.2 ± 0.4	

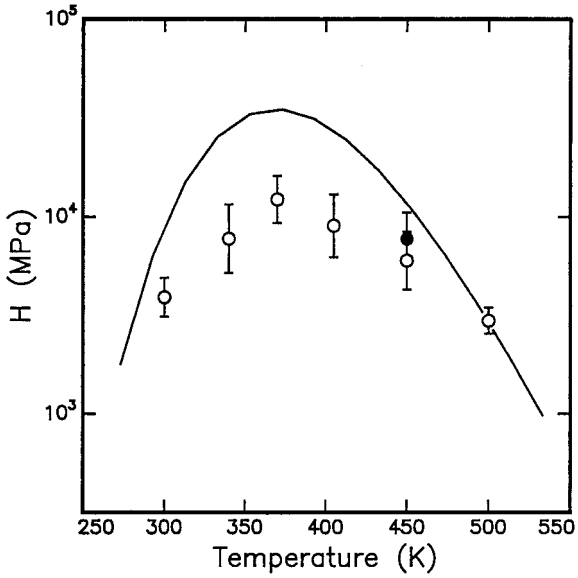

Figure 3. Henry's law constant of *n*-hexane in water. Experimental data (solid line)[23] and Monte Carlo simulation using the novel methodology that combines Widom insertion and EE techniques (points). Simulations using the Lorentz−Berthelot combining rules are shown as open symbols, and simulations using the Kong combining rules are shown as solid symbols.

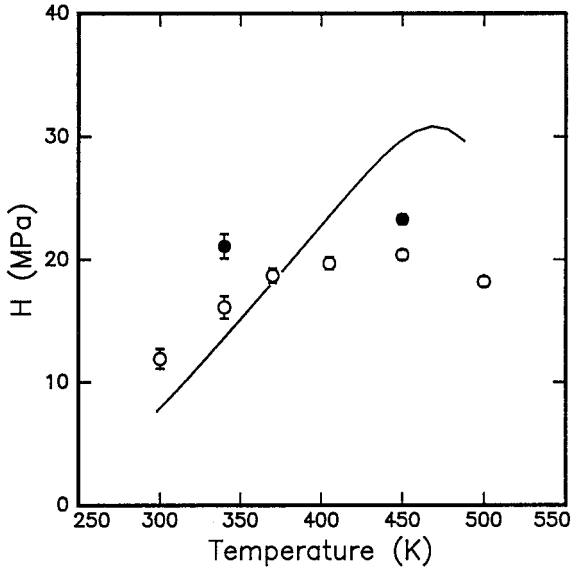

Figure 4. Henry's law constant of water in *n*-hexane. Experimental data (solid line)[23] and Monte Carlo simulation using the Widom insertion technique (points). Simulations using the Lorentz−Berthelot combining rules are shown as open symbols, and simulations using the Kong combining rules are shown as solid symbols.

potential predicts a much higher than actual permanent dipole moment for water that is not affected by the presence of hydrocarbon molecules. Furthermore, the pairwise potential does not account for the polar−induced polar interactions exhibited between water molecules and hydrocarbon molecules. These additional interactions affect considerably the structure of the mixture fluid and, as a result, the mixture phase equilibria in a complex way. Simulation results using the Kong combining rules do not seem to offer any substantial improvement.

To obtain a complete picture of the potential model capability for predicting the water−*n*-hexane mutual solubilities, the μ^{ex} value and the Henry's law constant of water in *n*-hexane was calculated through Widom insertions. Simulation results are presented in Table 4 and compared against experimental data in Figure 4. In this case, experimental data for the Henry's constant were obtained as follows: Experimental data for the water solubility in *n*-hexane[23] were fit to the NRTL activity coefficient model[24] in order to calculate the infinite dilution activity coefficient, which was subsequently used to estimate the Henry's constant, as prescribed by Tsonopoulos and Wilson.[23] The Henry's constant of water in *n*-hexane is much lower than the corresponding value of *n*-hexane in water at the same temperature, as a result of the much higher solubility of water in *n*-hexane. Simulation results are again in qualitative agreement with the experimental data. Calculations predict a smaller temperature dependence in the Henry's constant, resulting in considerable deviation at higher temperatures. Simulations using the Kong combining rules shift the Henry's constant to higher values without improving the overall accuracy. A thorough comparison between Lorentz−Berthelot and Kong combining rules in phase equilibrium predictions of different binary mixtures can found in the recent work of Potoff et al.[12]

Conclusions

The Henry's law constants of *n*-butane and *n*-hexane in water and of water in *n*-hexane were calculated using Monte Carlo simulation. A Buckingham exp-6 potential was used to calculate nonbonding interactions. The widely used Widom insertion technique for chemical potential calculations becomes inappropriate for relatively large solute molecules in dense solvents.

As a result, a novel methodology that combines Widom insertion and EE simulation was used for the case of *n*-butane and *n*-hexane in water. This methodology was shown to be very efficient and can be used for higher hydrocarbons.

The results presented in this work, combined with previous calculations for methane and ethane in water[13] and for cyclohexane and benzene in water,[10] reveal that the relatively simple pairwise potentials become progressively inaccurate for mixture predictions as the asymmetry in molecular size of unlike molecules increases. More complex potentials that account explicitly for polarizability and other many-body effects should be considered.

Acknowledgment. The work at the University of Maryland was supported by the National Science Foundation under Grant CTS-9509158. Partial financial support of this project from the NATO Collaborative Research Grants Program under Grant CRG 960966 is gratefully acknowledged.

References and Notes

(1) Panagiotopoulos, A. Z. *J. Phys. Condens. Matter* **2000**, *12*, R25.
(2) Boulougouris, G. C.; Economou, I. G.; Theodorou, D. N. *J. Phys. Chem. B* **1998**, *102*, 1029.
(3) Errington, J. R.; Panagiotopoulos, A. Z. *J. Phys. Chem. B* **1998**, *102*, 7470.
(4) Harris, J. G.; Yung, K. H. *J. Phys. Chem.* **1995**, *99*, 12021.
(5) Martin, M. G.; Siepmann, J. I. *J. Phys. Chem. B* **1998**, *102*, 2569.
(6) Nath, S. K.; Escobedo, F. A.; De Pablo, J. J. *J. Chem. Phys.* **1998**, *108*, 9905.
(7) Errington, J. R.; Panagiotopoulos, A. Z. *J. Phys. Chem. B* **1999**, *103*, 6314.
(8) Martin, M. G.; Siepmann, J. I. *J. Phys. Chem. B* **1999**, *103*, 4508.
(9) Spyriouni, D.; Economou, I. G.; Theodorou, D. N. *J. Am. Chem. Soc.* **1999**, *121*, 3407.
(10) Errington, J. R.; Panagiotopoulos, A. Z. *J. Chem. Phys.* **1999**, *111*, 9731.
(11) Spyriouni, D.; Economou, I. G.; Theodorou, D. N. *Phys. Rev. Lett.* **1998**, *80*, 4466.
(12) Potoff, J. J.; Errington, J. R.; Panagiotopoulos, A. Z. *Mol. Phys.* **1999**, *97*, 1073.
(13) Errington, J. R.; Boulougouris, G. C.; Economou, I. G.; Panagiotopoulos, A. Z.; Theodorou, D. N. *J. Phys. Chem. B* **1998**, *102*, 8865.
(14) Lyubartsev, A. P.; Martsinovski, A. A.; Shevkunov, S. V.; Vorontsov-Velyaminov, P. N. *J. Chem. Phys.* **1992**, *96*, 1776.
(15) Lyubartsev, A. P.; Laaksonen, A.; Vorontsov-Velyaminov, P. N. *Mol. Simul.* **1996**, *18*, 43.
(16) Lyubartsev, A. P.; Førrisdahl, O. K.; Laaksonen, A. *J. Chem. Phys.* **1998**, *108*, 227.
(17) Kong, C. L. *J. Chem. Phys.* **1973**, *59*, 2464.
(18) Buckingham, R. A. *Proc. R. Soc. London* **1938**, *168A*, 264.
(19) Allen, M. P.; Tildesley, D. J. *Computer Simulation of Liquids*; Clarendon Press: Oxford, 1987.
(20) Theodorou, D. N.; Suter, U. W. *J. Chem. Phys.* **1985**, *82*, 955.
(21) Frenkel, D.; Smit, B. *Understanding Molecular Simulation*; Academic Press: New York, 1996.
(22) Carroll, J. J.; Jou, F.-Y.; Mather, A. E. *Fluid Phase Equilib.* **1997**, *140*, 157.
(23) Tsonopoulos, C.; Wilson, G. M. *AIChE J.* **1983**, *29*, 990.
(24) Prausnitz, J. M.; Lichtenthaler, R. N.; de Azevedo, E. G. *Molecular Thermodynamics of Fluid Phase Equilibria*, 2nd ed.; Prentice-Hall: New York, 1986.